
IDENTIFICATION AND CORRECTION OF SAGNAC FREQUENCY VARIATIONS: AN IMPLEMENTATION FOR THE GINGERINO DATA ANALYSIS

A PREPRINT

Angela D.V. Di Virgilio and Umberto Giacomelli
INFN Sez. di Pisa,
Polo Fibonacci, Largo B Pontecorvo 3, I-56127 Pisa, Italy
angela.divirgilio@pi.infn.it

Nicolò Beverini, Giorgio Carelli, Donatella Ciampini, Francesco Fuso, and Enrico Maccioni
Università di Pisa,
Dipartimento di Fisica "E. Fermi", Largo B Pontecorvo 3, I-56127 Pisa, Italy

Antonello Ortolan
INFN-National Lab. of Legnaro, viale dell'Università 2, I-35020, Legnaro (PD), Italy

May 17, 2022

ABSTRACT

Ring laser gyroscopes are top sensitivity inertial sensors used in the measurement of angular rotation rates. It is well known that the response of such remarkable instruments can in principle access the very low frequency band, but the occurrence of nonlinear effects in the laser dynamics imposes severe limitations in terms of sensitivity and stability. We report here general relationships aimed at evaluating corrections able to effectively account for nonlinear laser dynamics. The so-derived corrections are applied to analyse thirty days of continuous operation of the large area ring laser gyroscope GINGERINO leading to duly reconstruct the Sagnac frequency ω_S . The analysis shows that, on the average, the evaluated corrections affect the measurement of the Earth rotation rate Ω_E at the level of 1 part in 1.5×10^3 . Among the identified corrections, the null shift term ω_{NS} is the dominant one. It turns out proportional to the optical losses μ of the ring cavity, which are changing in time at the level of 10% within the considered period of thirty days. The time behaviour is reconstructed based on available signals (interferogram and mono-beam intensities), and the Allan deviation of the estimated Ω_E shows a remarkable long term stability, leading to a sensitivity better than 10^{-10} rad/s with more than 10s of integration time, and approaching $(8.5 \pm 0.5) \times 10^{-12}$ rad/s with 4.5×10^5 s of integration time.

1 Introduction

Ring laser gyroscopes (RLGs) are inertial sensors based on the Sagnac effect [1, 2, 3]. They are largely used for inertial navigation, and applications in geodesy, geophysics and even for General Relativity tests are foreseen [4]. Since 2011 we are studying the feasibility of the test of Lense–Thirring dragging of the rotating Earth at the level of 1% with an array of large frame RLGs [5, 6, 7]. For that purpose it is necessary to push the relative accuracy of the Earth rotation rate Ω_E measurement in the range from 1 part in 10^9 up to 1 part in 10^{12} .

RLG consists of a laser with a cavity comprising of three or four mirrors, rigidly attached to a frame; large frame RLGs are utilised to measure the Earth rotation rate, being attached to the Earth crust. Because of the Sagnac effect, the two counter-propagating cavity modes have slightly different frequency, and the beat note of the two beams is proportional to the angular rotation rate of the ring cavity. Large frame RLGs are the most sensitive instruments for inertial angular rotation measurements. The Sagnac frequency of a RLG is in fact proportional to the component of the angular velocity $\vec{\Omega}$ felt by the instrument along the normal to the cavity plane:

$$f_s = S\Omega \cos \theta \quad (1)$$

$$S = 4 \frac{A}{\lambda L},$$

where A is the area of the ring cavity, L is its perimeter, λ the wavelength of the light, and θ is the angle between the area versor of the ring and $\vec{\Omega}$. For RLGs lying horizontally (area versor vertical) θ is the co-latitude angle, while for RLGs aligned at the maximum Sagnac signal $\theta = 0$. Eq. 1 defines the scale factor S , which is a function of the geometry and of λ , quantities that can be measured with a very high accuracy.

Further to sensitivity, other key points of such instruments rely on their broad bandwidth, which can span from kHz down to DC, and their very large dynamical range. In fact the same device can record microseismic events and high magnitude nearby earthquakes [8], being the signal based on the measurement of the beat note between the two counter-propagating beams. It has been proven that large size RLGs, equipped with state of the art mirrors, can reach the relative precision of 3 parts in 10^9 with one day of integration time, in the measurement of Ω_E [1]. If shot noise limited, sensitivity level scales with the square of the size of the ring cavity [1]. However, other limitations can affect the measurement. It is well known that the nonlinear laser dynamics plays a role in determining the RLG signal. We have recently developed a model to reconstruct the Sagnac frequency ω_S starting from the measured beat note ω_m and using the mono-beam signals¹. The Sagnac angular frequency can be expressed as the linear sum of

¹For mono-beam signals we intend the signals observed by the two photodiodes that detect the laser intensities in the counter-propagating directions.

six contributions. The first one, ω_{S0} , is dominant, it takes into account the so called back-scatter noise, as already discussed in [9].

In this paper we complete the analysis, providing the necessary information to evaluate the other terms. This analysis has been applied to thirty days of continuous operation of GINGERINO and the results are discussed. The so called null shift, ω_{NS} , is the dominant contribution after ω_{S0} . The main originality of this paper is the direct reconstruction of this term for RLG signals. It demonstrates that, differently from what assumed in previous approaches, the null shift affects not only accuracy, but also sensitivity of the apparatus, since it is linked to the optical losses μ , which depend on time.

2 Analysis

The present analysis starts from the model of the laser dynamics recently developed [9], based on the Aronowitz model of RLG [10, 11, 12], which describes the laser dynamics through several dimensionless parameters (Lamb parameters). The polarization of the laser plasma is described up to the third order expansion in power of the field [10, 12]. In the case of large frame RLG, to avoid mode competition, two Neon isotopes, ^{20}Ne and ^{22}Ne , are utilised, and the laser is set close to threshold to guarantee single-mode operation. This particular choice allows for some simplifications: the Lamb parameters of cross-saturation θ_{12} and θ_{21} can be neglected, and we can assume the self-saturation terms are equal each other, i.e., $\beta_1 = \beta_2 = \beta$. The model provides two analytical expressions for the Sagnac angular frequency: a non-linear relationship (eq. 8 of ref. [9]), which connects all the laser parameters with each other, and an approximate decomposition of ω_S as a linear sum of six terms, which is the collection of the first and second order expansion as a function of the two main terms:

$$\omega_S = \omega_{S0} + \omega_{NS1} + \omega_{NS2} + \omega_{K1} + \omega_{K2} + \omega_{\delta_{NS}K}. \quad (2)$$

In the present analysis only the first order terms of the Sagnac angular frequency are considered: $\omega_{NS1} = \omega_{NS}$, $\omega_{K1} = \omega_K$. A preliminary study has shown that the second order terms can be neglected, since too small compared with the present sensitivity of our prototype. The first term ω_{S0} does not require knowledge of the laser dynamics, and has been already illustrated in the previous paper [9]. Here we will report the detailed expressions to evaluate ω_{NS} and ω_K .

2.1 Implementation of the Model

To explicitly evaluate ω_{NS} and ω_K , the mono-beam signals are exploited [11, 12, 13]. We make use of the DC components, $PH1$ and $PH2$, of the monobeam signals, their AC components at the beat frequency $\omega_m/2\pi$, I_{S1} and I_{S2} , and the relative phase ϵ between the two AC components. Dissipative processes (like diffusion or absorption from the mirrors) can produce non reciprocal losses between the

two counter-propagating beams, so that two distinct loss parameters $\mu_1 \neq \mu_2$ must be used. Without loss of generality, it is possible to take $\mu_1 = \mu$ and $\mu_2 = \mu + \delta\mu$, where μ represents the reciprocal losses term and $\delta\mu$ the non reciprocal ones. The plasma dispersion function depends on several parameters: gas pressure, atomic characteristics of the two isotopes, line width of the excited atoms, resonance frequency of the two counter propagating modes, area of the beam profile at the discharge, and temperature of the plasma.

Assuming that $\beta_1 = \beta_2 = \beta$ (a rough evaluation reported in [11] gives $\beta_1 - \beta_2 \simeq 10^{-14}$), combining the information of the mono-beam DC signals $PH1$ and $PH2$ with the plasma dispersion function, the gains of the two beams $Gain1$ and $Gain2$ are evaluated. The non reciprocal loss term $\delta\mu$ is hence determined.

Using other relationships reported in the literature [13] it is possible to write ω_{NS} and ω_K as a function of the known quantities ω_m , $PH1$, $PH2$, I_{S1} , I_{S2} , ϵ , and μ . μ can be evaluated off-line with 1% precision by measuring the ring down time of the cavity. The analytical calculation shows that μ is a multiplicative factor in ω_{NS} , which accordingly can be evaluated by means of a best fit. The term ω_{NS} depends on μ , $\delta\mu$, $PH1$, $PH2$, I_{S1} and I_{S2} , and decreases linearly for increasing perimeter length L . It exhibits also a small modulation as a function of ϵ , according to: $\frac{1}{2} \times (1 + \frac{I_{S1}I_{S2} \cos(2\epsilon)}{2PH1PH2})^{-1/2} + \frac{1}{2}$, where $\frac{I_{S1}I_{S2}}{PH1PH2} \ll 1$. The best case is when $\delta\mu = 0$, leading, with the parameters of GINGERINO, to $\omega_{NS} \simeq 10 \mu\text{rad/s}$, which gives $\omega_{NS} \sim 2\text{mrad}$ assuming $\mu = 2 \times 10^{-4}$. In such conditions, the amplitude of the modulation induced by the $\cos(2\epsilon)$ term is in the nHz range. In this best case the null shift term is about 1 part in 10^6 of Ω_E , but its fluctuations are no larger than 1 part in 10^{11} . A similar evaluation on the presently available data of GINGERINO leads to $\delta\mu = 0.02\mu$, $\omega_{NS} \sim 1\text{rad/s}$, with a modulation due to the $\cos(2\epsilon)$ term of $10 \mu\text{rad/s}$.

The evaluation of ω_K requires some further assumptions. ω_K oscillates at the Sagnac frequency, containing $\sin(\omega_{St})$ and $\cos(\omega_{St})$ terms. However, due to non-linear dynamics, the long time average of such oscillating terms can deviate from zero. Therefore, we can express ω_K as the product of a small parameter MK with a given function of known parameters. The value of MK and its very slow variations can be found by a best fit procedure.

In the appendix, a Mathematica notebook is reported showing the details of the symbolic calculations leading to ω_{NS} and ω_K functions, and the estimation of the required parameters. We note that, according to our model, ω_K can be written as the ratio of two polynomials where the parameter μ enters in one term, preventing direct evaluation of such a parameter through a simple fit procedure. However, we have checked that, with typical μ values of 100 – 1ppm, variations in calculated results are not significant.

In the following, we report the calculations for a general RLG dynamics, and their implementation for the specific

case of GINGERINO.

2.2 The selected playground and the first step of the analysis

Thirty days of continuous operation between June 16 and July 15 2018 have been selected for this test. After June 21, heavy operations took place in the underground laboratories where GINGERINO is placed for the building of another experiment. Disturbances induced in GINGERINO operation are well visible in the second half of the data stream. We included also these data to show that, even in non ideal conditions, very high sensitivity and stability can be obtained. The data are acquired with our DAQ system at 5kHz sampling rate[14]. The whole set of data has been analysed on a hourly base, and the terms ω_m , ω_{NS} (with $\mu = 1$), ω_ξ (with $\xi = 1$), and ω_K (with $MK = 1$ and $\mu = 10^{-4}$) evaluated and stored for offline analysis. In the calculation, average losses $\mu = 10^{-4}$ are used to evaluate ω_K , since it has been checked that the dependence on μ is negligible at the present sensitivity limit. The analysis, based on the Hilbert transform of interferograms and mono-beam intensities, leads to the beat note frequency $\omega_m/2\pi$, the amplitudes of the mono beams at the beat frequency I_{S1} , I_{S2} , and the relative phase ϵ . In order to avoid spurious oscillations due to the boundaries between contiguous hours in the hourly-based analysis, for each hour 6 minutes of data are added at the beginning and at the end; these extra samples are removed after the analysis (overlap-save method). The analysed data are stored after decimation at 20 and 0.1Hz; the decimation is implemented via the standard Matlab function `decimate`, which applies 8th order Chebyshev Type I lowpass filter with cutoff frequency $0.8 \times (Fs/2)$, where Fs is 20 or 0.1Hz.

2.3 The second step of the offline procedure

A second routine collects different days for longer analysis. The first operation is to identify the portions of data which are not at normal operation, typically less than 5 % of the data are removed. To this aim, we make use of the fringe contrast of the interferogram acquired at 20Hz rate. The choice of such a sampling rate minimizes the discarded sample. This operation associates the flag 1 to the good samples and the flag 0 to the bad ones; from this routine we get the mask to select data decimated at lower frequency. In the present analysis, decimated at half an hour rate, 90% of data are selected. Both the intensity of the mono-beam signal ($PH2$), that is not used for the feedback control of the laser operation, and of the Discharge Monitor (DM , i.e. a photodiode looking at the laser discharge) change with time. This is a clear indication that μ changes with time; in particular, $PH2$ indicates the presence of non reciprocal losses $\delta\mu$, while DM is proportional to the total excited atoms, and therefore to the total losses. DM and $PH2$ signals allow us to model the change of losses as a function of time through two form factors,

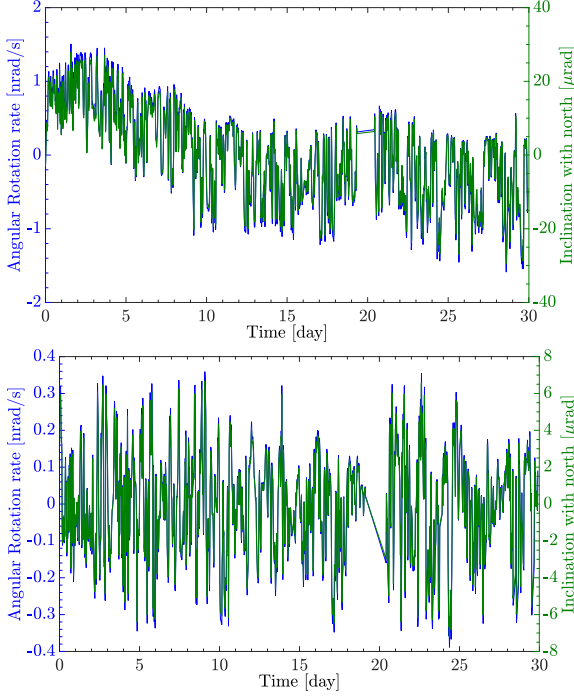


Figure 1: Top: Time variations expressed as Ω and θ , see Eq. 2, of the analysed data [utilising ω_{S0} with the mean value subtracted; the mean value is $2\pi \times (280.208 \pm 0.001\text{Hz})$, compatible with a RLG with area versor vertical with a few mrad error]. Bottom: as above, but using ω_S evaluated with the linear regression model.

- gain monitor form factor: $FF_{DM} = \frac{DM - \langle DM \rangle}{\langle DM \rangle}$
- mono-beam 2 form factor: $FF_{PH2} = \frac{\langle PH2 - \langle PH2 \rangle \rangle}{\langle PH2 \rangle}$.

2.4 Reconstruction of the Sagnac frequency by a linear regression model

The vectors ω_{NS} , $\omega_{NS} \times FF_{DM}$, $\omega_{NS} \times FF_{PH2}$, ω_ξ , and ω_K are collected, and the linear regression method is utilised to determine the unknown parameters μ , MK and ξ , and evaluate ω_S accordingly.

Let us remind that ω_{S0} accounts for back scatter noise, and an additional term ω_ξ has been implemented to account for inaccuracies on the measured quantities $I_{S1,2}$, $PH_{1,2}$ and ϵ [9]. In summary, in the procedure μ and MK are physical quantities which could be evaluated independently, while ξ compensates noises in the measured quantities.

Fig. 1 shows data before (top panel) and after (bottom panel) the application of this procedure. The dispersion across the mean value is clearly suppressed using ω_S , meaning that the new regressive analysis, which includes the terms ω_{NS} and ω_K , duly accounts for it. The Matlab function *lm2* has been used to perform linear regression. Results indicate that the p-value, which tests the null hypothesis, is approximately zero for all vectors excluding

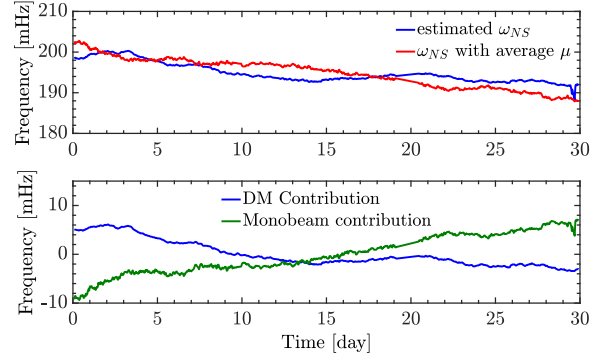


Figure 2: Top: the best-fit evaluated ω_{NS} and the one calculated assuming average losses. Bottom: the contribution using the *DM* and *PH2* to follow the time behaviour of the losses μ .

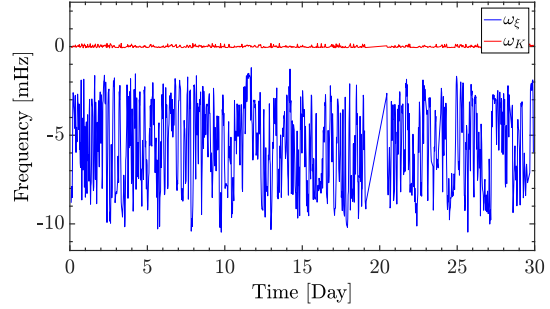


Figure 3: The first step of the analysis evaluates ω_{S0} , which accounts for back-scatter noise; ω_ξ has been developed to further improve back-scatter cancellation, taking into account inaccuracies in the signals *PH1*, *PH2*, $I_{S1,2}$ and ϵ .

the one related to ω_K , whose p-value is 0.038. On the other hand, the relative error in the estimation of the *MK* term involved in the ω_K expression is around 50%, whereas it amounts to 1 – 12% for all other vectors.²

Fig. 2 shows the contribution of the laser systematics. A dominant role is played by ω_{NS} , which produces a slowly variable level ranging between 180 – 200mHz, with standard deviation 2.3mHz. ω_ξ gives a small correction with mean value -5.7mHz and standard deviation 2.3mHz. These two terms affect residuals, whereas ω_K is smaller by more than a factor 10; it has a mean value compatible with zero and standard deviation 0.05mHz, see Fig. 3.

Fig. 4 shows the evaluated losses. During the 30 day period considered, a variation of 12% is observed in μ , with a visible trend towards higher losses for increasing time. Fig. 5 compares the distributions of the beat frequency

²The coefficient of determination of the linear regression procedure and the standard deviation of the obtained residuals are $R^2 = 0.952$ and $770 \pm 3\mu\text{Hz}$, respectively.

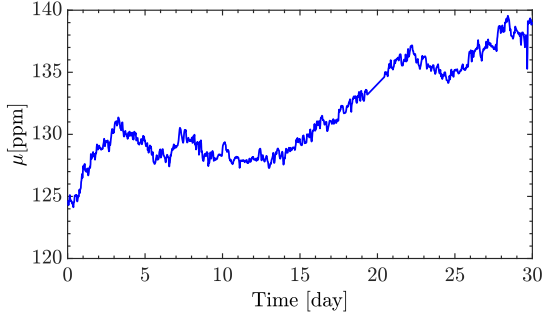


Figure 4: Time behaviour of the losses, estimated with the *DM* and the uncontrolled monobeam signal *PH2*.

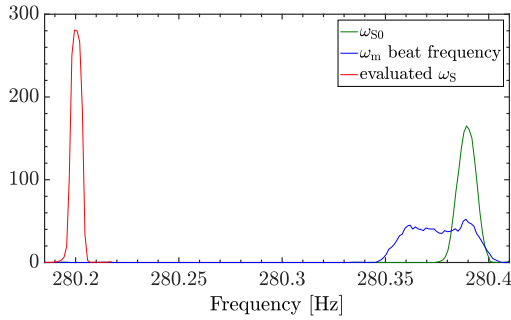


Figure 5: Distribution of the beat frequency $\omega_m/2\pi$, of the first stage of the reconstruction $\omega_{S0}/2\pi$ and of the final $\omega_S/2\pi$.

$\omega_m/2\pi$, of the $\omega_{S0}/2\pi$ reconstructed in the first stage of our approach and that of the finally determined $\omega_S/2\pi$. It should be noticed that the distribution of ω_m is highly non-Gaussian while that of both reconstructed frequencies becomes close to Gaussian, demonstrating that the nonlinear terms of dynamics are correctly accounted for. Moreover, ω_S is shifted towards lower frequencies as a consequence of the null shift term ω_{NS} .

Fig. 6 reports the modified Allan deviation, expressed in angular rotation rate. We observe that, after the application of the procedure (red line), the variance is decreasing with the integration time up to more than two days. This suggests that with our procedure we are effectively correcting the long term laser dynamic effects. It is well known that RLGs are sensitive to Chandler Wobbler effect, which is typically below 100nrad. We have checked that the level reached in the long term stability is above the limit imposed by the Chandler Wobbler effect. The so far obtained long term instability is about 10 times larger than the scale factor changes induced by temperature variations considering $5 \times 10^{-6}/^\circ\text{C}$ the thermal expansion coefficient of granite, the material used for the RLG frame, and 0.02°C as typical temperature variation in the 30 day period. The obtained modified Allan deviation represents a fair improvement compared to the analysis in [14], carried out by

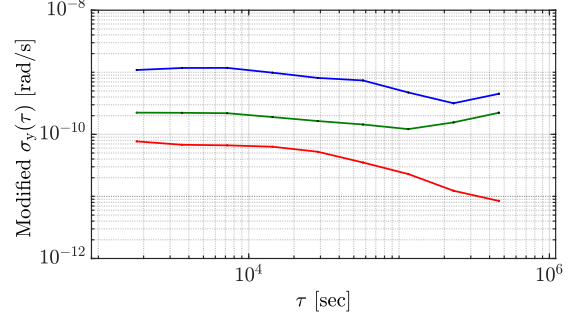


Figure 6: Modified Allan deviation of the measured angular velocity Ω from the beat note (ω_m), ω_{S0} and evaluated ω_S (blue, green and red lines, respectively), relative to the mean value, expressed in angular velocity [rad/s].

using available signals on a pure phenomenological basis, for instance the long time behaviour was cancelled using the *DM* signal.

3 Discussion and Conclusions

The Sagnac frequency ω_S of the GINGERINO RLG has been evaluated taking into account the laser dynamics. The model leads to a linear sum of several terms, which can be determined with the available signals of beat frequency and mono-beams. The so-called back-scatter noise, which has been so far considered the most severe limitation of RLG, is accounted for by terms ω_{S0} and ω_ξ . It turns out that the null shift term ω_{NS} is the second dominant contribution. It depends linearly on cavity losses μ ; this term definitely affects accuracy of the apparatus, since in the best case, if the losses are constant, it represents a non-negligible DC contribution. Furthermore, it is likely that losses are not constant with time, hence ω_{NS} affects stability. If a long term stability of 1 part in 10^9 is required for the Ω_E measurement, the requirement for the stability of μ with time, or equivalently for the relative accuracy in the evaluation of μ , is $\frac{\omega_{NS}}{\omega_S} \times 10^9$. According to the model, it is straightforward to see that the null shift level is minimised when $\delta\mu \simeq 0$.

Changes of μ at the level of 10% are evident in GINGERINO. In order to follow those changes we have utilised the DC mono-beam signal of the uncontrolled beam, that is the signal which is not used in feedback loops controlling the laser operation (beam 2 in our case), and the discharge monitor *DM*, also called gain monitor. ω_S is evaluated with a linear regression model, see Eq. 2.

Remarkably, during the measurements considered in this paper, in particular after the twentieth day of the 30 day record, heavy activity was present for the construction of a new experiment inside the underground laboratory hosting the RLG. Despite that, and the fact that GINGERINO is not equipped with control of the geometrical scale factor (accordingly its wavelength is not fixed), in 5.4 days of integration time it has reached the relative stability of

$(1.7 \pm 0.07) \times 10^{-7}$ [corresponding to a resolution in the angular velocity measurement of $(8.5 \pm 0.5) \times 10^{-12}$ rad/s]. The analysis poses the problem of the accuracy of angular velocity estimations; however, it is not straightforward to understand the accuracy of the final measurement, an issue to be addressed by future Monte Carlo studies.

The analysis has also shown that losses are the main limitation of GINGERINO. The question is now which part of the apparatus is the main responsible for losses and for their behaviour as a function of time. The hypothesis is that the main contribution comes from the gain tube of the laser. In the standard high sensitivity RLG scheme, it acts as gain tube and as spatial filter. The laser discharge is in fact produced within a pyrex capillary, with inner diameter of 4 mm, which is a bit small compared to the waist of the beams.

In the near future, a new capillary tube with slightly larger inner diameter will be installed in GINGERINO to limit losses. Furthermore, additional data, such as current of the discharge tube and laser wavelength, will be continuously recorded in order to better characterise the instrument operation in the long term.

As far as the analysis is concerned, the effect of terms $\theta_{1,2}$ will be included in the model. The data analysis will be extended in order to evaluate the null shift second order term ω_{NS2} and to better understand the influence of each parameter, in particular of the change of wavelength in the RLG operation, which for the present set of data matters since GINGERINO is free running and the wavelength can change with even small temperature variations.

References

- [1] Karl Ulrich Schreiber and Jon-Paul R. Wells. Invited review article: Large ring lasers for rotation sensing. *Review of Scientific Instruments*, 84(4):041101, 2013.
- [2] The Sagnac effect: 100 years later. *Comptes Rendus Physique*, 15(10):iii – iv, 2014. Alexandre Gauguier, Editor.
- [3] Angela Di Virgilio, Maria Allegrini, Alessandro Beghi, Jacopo Belfi, Nicolo Beverini, Filippo Bosi, Bachir Bouhadeh, Massimo Calamai, Giorgio Carelli, Davide Cuccato, Enrico Maccioni, Antonello Ortolan, Giuseppe Passetto, Alberto Porzio, Matteo Luca Ruggiero, Rosa Santagata, and Angelo Tartaglia. A ring lasers array for fundamental physics. *Comptes Rendus Physique*, 15(10):866 – 874, 2014. The Sagnac effect: 100 years later / L'effet Sagnac : 100 ans après.
- [4] Monika Tercjak and Aleksander Brzeziński. On the influence of known diurnal and subdiurnal signals in polar motion and ut1 on ring laser gyroscope observations. *Pure and Applied Geophysics*, 2017.
- [5] F. Bosi, G. Cella, A. Di Virgilio, A. Ortolan, A. Porzio, S. Solimeno, M. Cerdonio, J. P. Zendri, M. Allegrini, J. Belfi, N. Beverini, B. Bouhadeh, G. Carelli, I. Ferrante, E. Maccioni, R. Passaquietti, F. Stefani, M. L. Ruggiero, A. Tartaglia, K. U. Schreiber, A. Gebauer, and J-P. R. Wells. Measuring gravitomagnetic effects by a multi-ring-laser gyroscope. *Phys. Rev. D*, 84:122002, 2011.
- [6] Angelo Tartaglia, Angela Di Virgilio, Jacopo Belfi, Nicolo Beverini, and Matteo Luca Ruggiero. Testing general relativity by means of ring lasers. *The European Physical Journal Plus*, 2017.
- [7] Angela D. V. Di Virgilio, Jacopo Belfi, Wei-Tou Ni, Nicolo Beverini, Giorgio Carelli, Enrico Maccioni, and Alberto Porzio. Ginger: A feasibility study. *The European Physical Journal Plus*, 2017.
- [8] A Simonelli, H Igel, J Wassermann, J Belfi, A Di Virgilio, N Beverini, G De Luca, and G Saccorotti. Rotational motions from the 2016, central italy seismic sequence, as observed by an underground ring laser gyroscope. *Geophysical Journal International*, 214(1):705–715, 2018.
- [9] Angela D.V. Di Virgilio, Nicolo Beverini, Giorgio Carelli, Donatella Ciampini, Francesco Fuso, and Enrico Maccioni. Analysis of ring laser gyroscopes including laser dynamics. 2019.
- [10] F. Aronowitz and R. J. Collins. Lock-in and intensity-phase interaction in the ring laser,. *Journal of Applied Physics*, 41:1, 1970.
- [11] Alessandro Beghi, Jacopo Belfi, Nicolo Beverini, B. Bouhadeh, D. Cuccato, Angela Di Virgilio, and Antonello Ortolan. Compensation of the laser parameter fluctuations in large ring-laser gyros: a kalman filter approach. *Appl. Opt.*, 51(31):7518–7528.
- [12] D. Cuccato, A. Beghi, J. Belfi, N. Beverini, A. Ortolan, and A. Di Virgilio. Controlling the nonlinear inter cavity dynamics of large he-ne laser gyroscopes. *Metrologia*, 51:97–107, 2014.
- [13] Davide Cuccato. *Modeling, estimation and control of ring Laser Gyroscopes for the accurate estimation of the Earth rotation*. PhD thesis, University of Padova, 2016.
- [14] J. Belfi, N. Beverini, G. Carelli, A. Di Virgilio, U. Giacomelli, E. Maccioni, A. Simonelli, F. Stefani, and G. Terreni. Analysis of 90 day operation of the gingerino gyroscope. *Appl. Opt.*, 57(20):5844–5851.

Appendix A: Identification of He-Ne Ring Laser dynamics

Reference papers:

F. Aronowitz and R. J. Collins, J. Appl. Phys. 41, 1 (1970).
 A. Beghi, J. Belli, N. Beverini, B. Bouhadef, D. Cuccato, A. D. Virgilio, and A. Ortolan, Appl. Opt. 51, 7518 (2012).
 D. Cuccato, A. Beghi, J. Belli, N. Beverini, A. Ortolan, and A. D. Virgilio, Metrologia 51, 97 (2014).
 Master thesis of Davide Cuccato: http://www.infu.it/thesis/thesis_dettaglio.php?tid=10072
 PhD thesis of Davide Cuccato: http://www.infu.it/thesis/thesis_dettaglio.php?tid=6109

Constants and parameters of He-Ne Ring Lasers

Beam = Cw, Beam + = Ccw, Isotope 1 = Ne20, Isotope 2 = Ne22

```

c = 299792458 (* speed of light m/s *)
h = 6.62606996 * 10^-34 (* Planck constant Js *)
e0 = 8.854187817 * 10^-12 (* Fundamental dielectric constant F/m *)
lambda = 632.81 * 10^-9 (* He-Ne laser wavelength m *)
kB = 1.3806488 * 10^-23 (* Boltzmann constant J/K *)
u = 1.660538921 * 10^-27 (* unified atomic mass unit kg *)
SF = L/lambda/4 (* Scale factor of the instrument *)
(*area= 0.52*0.73*10^4
(* area of the transverse section of the beam m^2 *)*)
FSR = c/L (* Cavity finesse or Free spectral range Hz *)
(*FS= 280.4 (* Sagnac frequency Hz GINGERINO *)*)
FS = X + SF; (*detuning, in function of the bias,
general, X is the angular velocity bias of the RL6*)
ya = (8.35 + p) 10^6 (* Decay rate of level a *)
yb = (9.75 + 4p) 10^6 (* Decay rate of level b *)
Aik = 3.39 * 10^6 (* Transition rate between laser levels *)
yab = (ya + yb) / 2 + dy
(* Radiation decay rate plus collision induced rate *)
dy = 0;
m20 = 20 u (* atomic mass isotope 1 *)
m22 = 22 u (* atomic mass isotope 2 *)
k20 = 1/2 (* Relative concentration of isotope 1 *)
k22 = 1/2 (* Relative concentration of isotope 2 *)
rD20 = (sqrt(kB 350 * (1 + V) / m20) / lambda) (* Doppler halfwidth isotope 1 rad/s *)
rD22 = (sqrt(kB 350 * (1 + V) / m22) / lambda) (* Doppler halfwidth isotope 1 rad/s *)
V = 0;

```

2 | Appendix_A.nb

```

muab = sqrt(pi * e0 * Aik * (lambda / (2 * pi))^3 * h) (* Electric dipole moment
of the transition 0.95+1.6022*10^-19+0.0053*10^-9 *)
n20 = yab / rD20 (* homogeneous to doppler broadening rate isotope 1 *)
n22 = yab / rD22 (* homogeneous to doppler broadening rate isotope 2 *)
Sh = 885 * 10^6 (* isotopic shift Hz *)
e120 = (0 + Sh / 2) / rD20
(* Detuning normalized to Doppler width for beam 1, isotope 1 *)
(*Clockwise*)
e220 = (fs + Sh / 2) / rD20
(* Detuning normalized to Doppler width for beam 2, isotope 1 *)
(*CounterClockwise*)
e122 = (0 - Sh / 2) / rD22
(* Detuning normalized to Doppler width for beam 1, isotope 2 *)
e222 = (fs - Sh / 2) / rD22
(* Detuning normalized to Doppler width for beam 2, isotope 2 *)
cI2P = (pi^2 * muab^2 / (2 * h^2 * ya * yb * 2 * e0 * T * a))
(* Calibration Constant from Power to Lamb Units *)

```

Electronic constants to express all in function of the monobeams voltage

```

cI2V = cI2P / Gamp / aEff
(* Calibration Constant from Acquired Voltage to Lamb Units *)

```

Evaluation of output power and mean intensities from the above constants

```

Pout = Vsamp / Gamp / aEff (* Output power 1-10 nW *)
ImeanP = cI2P * Pout (* Check Mean intensity in Lamb units *)
ImeanV = cI2V * Vsamp (* Check Mean intensity in Lamb units *)

```

Plasma dispersion function

```

Zi[e_-, n_] = sqrt(pi) * e^-e^2 - 2 * n;
(* Imaginary part of the plasma dispersion function *)
Zr[e_-, n_] = -2 * e * e^-e^2; (* Real part of the plasma dispersion function *)
L[e_-, n_] = 1 / (1 + (e/n)^2) (* Lorentzian function *)

```

Lamb Parameters expressions for the single isotope case

```

beta[e_-, n_-, G_] = G * (Zi[e_-, n_] / Zi[0, n_]) (*Self saturation coefficient *)
os[e_-, n_-, G_-, mu_] = beta[e_-, n_-, G] - mu
(* Excess of gain minus losses coefficients *)
os[e_-, n_-, G_] = G * (FSR * Zr[e_-, n_] / (2 * Zi[0, n_]))
(*Scale Factor error coefficient due to laser physics *)
os[eX_-, eY_-, n_-, G_] = beta[eY, n_-, G] * L[eX, n_]
(*Cross saturation coefficient *)
ts[eX_-, eY_-, n_-, G_] = G * (FSR * (eX / lambda) * (Zi[eY, n_] / Zi[0, n_]) * L[eX, n_])
(* Null shift error coefficient *)

```

Lamb Parameters expressions for the double isotope case

20 and 22 are the isotopes; X and Y are the counter-propagating beams

```

beta[e20_-, e22_-, nu20_-, nu22_-, G_] = k20 * beta[e20, nu20, G] + k22 * beta[e22, nu22, G];
ad[e20_-, e22_-, nu20_-, nu22_-, G_-, mu_] =
k20 * os[e20, nu20, G, mu] + k22 * os[e22, nu22, G, mu];
od[e20_-, e22_-, nu20_-, nu22_-, G_] = k20 * os[e20, nu20, G] + k22 * os[e22, nu22, G];
od[eX20_-, eX22_-, eY20_-, eY22_-, nu20_-, nu22_-, G_] =
k20 * os[eX20, eY20, nu20, G] + k22 * os[eX22, eY22, nu22, G];
td[eX20_-, eX22_-, eY20_-, eY22_-, nu20_-, nu22_-, G_] =
k20 * ts[eX20, eY20, nu20, G] + k22 * ts[eX22, eY22, nu22, G];

Gain2 =
Simplify[NSolve[ImeanP == ad[e220, e222, n20, n22, G, mu + delta] / beta[e220, e222,
n20, n22, G], G][[1, 1, 2]] /. VsampLd -> PH2];
Gain1 = Simplify[NSolve[ImeanP == ad[e120, e122, n20, n22, G, mu] /
beta[e120, e122, n20, n22, G], G][[1, 1, 2]] /. VsampLd -> PH1];

beta1 = Simplify[beta[e120, e122, n20, n22, Gain1] /. VsampLd -> PH1];
beta2 = Simplify[beta[e220, e222, n20, n22, Gain2] /. VsampLd -> PH2];
DM = Solve[beta1 == beta2, delta]; DMU = delta /. DM[[1, 1]];
beta = beta1;

```

Evaluating Lamb Parameters

```

o1 = Simplify[od[e120, e122, n20, n22, Gain1]];
o2 = Simplify[od[e220, e222, n20, n22, Gain2]];
t12 = Simplify[td[e120, e122, e220, e222, n20, n22, Gain1]];
t21 = Simplify[td[e220, e222, e120, e122, n20, n22, Gain2]];

```

4 | Appendix_A.nb

omegaNS evaluation

```

omegaNS = Simplify[omega2 - omega1 + c21 * PH2 - c12 * PH1];
omegaNS = -omegaNS (um / 2 / Sqrt[8 * c^2 * r1 * r2 * Cos[2 * e] / L^2 + um^2] + 1/2);

```

K approximation and omegaK evaluation

```

K = Sqrt[a1 / a2] * c * r1 + (-Cos[e] Sin[tus] + Cos[tus] Sin[e]) -
Sqrt[a2 / a1] * c * r2 (Cos[e] Sin[tus] + Cos[tus] Sin[e]);

```

Assuming <Cos[e]> = <Sin[e]> = MK, where MK is a proportionality constant estimated by statistics

```

omegaK = MK * (sqrt(a1/a2) * IS2 * L * um * (-Cos[e] + Sin[e]) - sqrt(a2/a1) * IS1 * L * um * (Cos[e] + Sin[e])) /
(4 * sqrt(PH1 * PH2) - 4 * sqrt(PH1 * PH2));

```

```

omegaK = K / L * (-um / 2 / Sqrt[8 * c^2 * r1 * r2 * Cos[2 * e] / L^2 + um^2] - 1/2);

```

Calculations of alpha12 and r12 parameters

```

alpha1 = beta (PH1 + IS1^2 * 4 / PH1) + IS1 * IS2 * um * Sin[2 * e] / PH2 * 4 / (c / L);
alpha2 = beta (PH2 + IS2^2 * 4 / PH2) - IS1 * IS2 * um * Sin[2 * e] / PH1 * 4 / (c / L);
r1 = IS2 * um / 2 / (c / L) / Sqrt[PH1 * PH2] / 2;
r2 = IS1 * um / 2 / (c / L) / Sqrt[PH1 * PH2] / 2;

```

Operation Parameters of GINGERINO

```

p0 = 4.66 (* Gas pressure mbar *)
p = p0 / 1.33 (* Gas pressure Torr *)
a = pi * 0.52 * 0.73 * 10^-6; (*area of the mode*)
T = 0.35 * 10^-6 (* Mirror transmission coefficient *)
L = 4 * 3.60 (* Perimeter of the Ring m *)
aEff = 0.4 (* photodiode quantum efficiency *)
Gamp = 10^9 (* Transimpedance amplifier gain *)
X = 280.4 / SF; (*mean value of the angular velocity, rad/s*)

```

Calculation of functions to be implemented in the analysis

```

FunuNS[um_-, e_-, PH1_-, PH2_-, mu_-, delta_] = Simplify[omegaNS];
FunuK[um_-, e_-, PH1_-, PH2_-, IS1_-, IS2_-, mu_-, MK_] = Assuming[um > 0, Simplify[omegaK]];

```